ACS APPLIED MATERIALS & INTERFACES

Forum Article

www.acsami.org

Photoresponse of Donor/Acceptor Blends in Organic Transistors: A Tool for Understanding Field-Assisted Charge Separation in Small Molecule Bulk Heterojunction Solar Cells

Yuan Zhang, Jianhua Liu, and Thuc-Quyen Nguyen*

Center for Polymers and Organic Solids, Department of Chemistry and Biochemistry, University of California, Santa Barbara, Santa Barbara, California 93106, United States

Supporting Information

ABSTRACT: Photoresponse and ambipolar charge transport in organic bulk heterojunctions (BHJ) is investigated using field-effect transistors (FET) based on two donors, poly(3-hexylthiophene) (P3HT) and 3,6-bis(5-(benzofuran-2-yl)thiophen-2-yl)-2,5-bis(2-ethylhexyl)pyrrolo[3,4-c]pyrrole-1,4-dione (DPP(TBFu)$_2$) blends with [6,6]-phenyl-C70-butyric acid methyl ester ($PC_{70}BM$) acceptor. Upon 100 mW/cm^2 AM 1.5 G illumination, P3HT:$PC_{70}BM$ shows an equivalent hole and electron current together with a largely enhanced photoresponse in the FET. The DPP(TBFu)$_2$:$PC_{70}BM$ blends display an electron-dominating transport along with showing a relatively poor photoresponse in FETs upon irradiation. By comparing the two systems, it suggests that DPP(TBFu)$_2$:$PC_{70}BM$ possesses a less-efficient charge separation assisted by electric fields after exciton dissociation. The FET results correlate well to the solar cell device performance and provide further understanding and optimizing of solution-processed DPP small molecule solar cells.

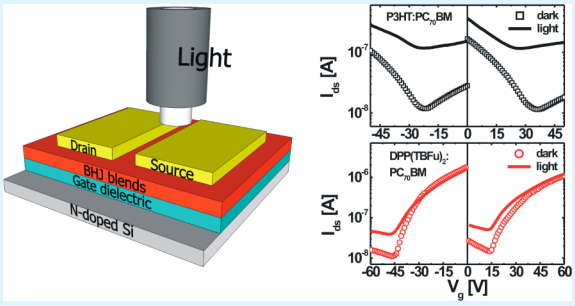

KEYWORDS: *bulk heterojunction, photocurrent, fill factor, field-effect transistor, charge separation*

1. INTRODUCTION

Solution-processed bulk heterojunction (BHJ) solar cells using small molecule donor materials are great alternatives to polymer photovoltaic devices,[1−6] because of their advantages concerning ease of purification and well-defined chemical structure when compared to polymeric systems.[7−10] Power conversion efficiencies (PCEs) of solution-processed SMBHJ solar cells up to 7% have been reported.[11−17] Small molecules incorporating diketopyrrolopyrrole (DPP) moiety with a strong electron withdrawing ability have been used as donors for solution-processed SM-BHJ solar cells with PCE of 4.8% and field-effect mobilities of 1×10^{-2} cm^2/(V s).[18,19] However, the PCEs of these devices are often limited by a relatively low fill factor (*FF*) that typically falls in a range of 0.4−0.5. Reasons for the reduced *FF*s in BHJ solar cells are still not fully understood and it can often be correlated to imbalance charge transport properties or strong recombination.[20−25] The nongeminate and geminate recombination losses in small molecule BHJs have been quantified using electrical transient measurements.[26] Recently, the field dependence of the recombination process has been evaluated using impedance spectroscopy, and the strength of field dependence well-correlates with the *FF*s in a series of small molecule BHJ solar cells.[27] Due to the strong Coulombic interaction in organic semiconductors, dissociated charge carriers after the splitting of excitons may not be totally free and are like to be bound electron−hole pairs.[21,28] It is generally considered that the creation of free carriers and the charge separation can be assisted by the electric field (E) or temperature.[29−33] In BHJ solar cells, the E is changed with the bias and a large E dependence of the charge separation would be likely to affect the photocurrent and the *FF*. Therefore, investigation of the field-assisted charge separation is informative to enable a more in-depth understanding of the *FF* and the ultimate solar cell performance.

Organic field-effect transistors (OFETs) have been wildly used to characterize the charge transport in pristine semiconductors[34] and donor/acceptor solar cell BHJ blends.[35] Although there is a difference in the charge transport direction in the OFET and solar cell, adopting OFET analysis is advantageous in a way that the electron and hole transport in the BHJs can be independently characterized on a single device using different gate voltage. Specifically, it is possible to utilize OFETs to explore the charge separation in BHJ blends by measuring the photoresponse. The field dependence of this process can be evaluated by varying the bias or the resultant E during the OFET operation. Quantitative determination of the vertical distribution of E in the OFET is challenging and therefore there is an uncertainty of E regarding the strength and

Special Issue: Forum on Advancing Technology with Organic and Polymer Transistors

Received: November 25, 2012
Accepted: February 8, 2013
Published: February 22, 2013

distribution of field across the active layer. However the lateral distribution of E as a function of distance from the source-drain electrodes has been probed experimentally using Kelvin probe.[36,37] The electric potential close to the contacts is found to have a very sharp gradient than the position in the middle of OFET channel. Furthermore, a direct probe of the electric field using microscopic second-harmonic generation[38,39] shows an E in the OFET that exhibits power-decay with distance from the drain contact (in the off-state) or from the source contact (in the on-state). The E is mostly concentrated in an area extended with 2−3 μm from the contact (for a channel width of 30 μm).

Figure 1 shows a schematic illustration for an OFET operated in different modes. For the ease of analysis, we

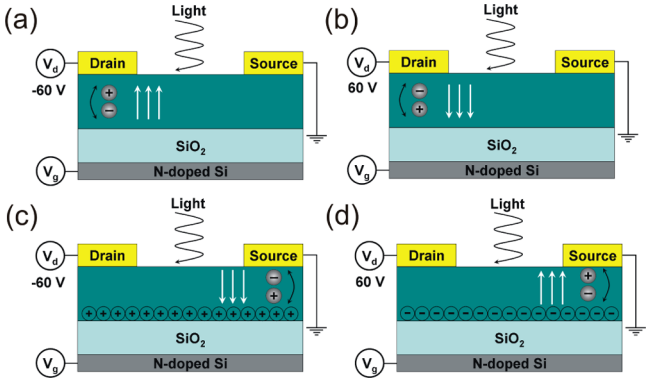

Figure 1. Schematic illustration of an ambipolar FET with photoactive layers upon irradiation when operated at (a) hole and (b) electron accumulation modes, respectively with low gate bias (turn-off). (c, d) According FET operations at hole and electron accumulation modes with high gate bias (turn-on).

assume an average vertical E generated in the OFET under operation as depicted by the white arrows in Figure 1. The simplification of E is can be supported by the experimental results reported previously.[31,33] Depending on the gate bias (V_g), under both the p-type and n-type modes, the E created in the OFET will be stronger in the area laterally near the drain or the source electrodes when applying a low V_g or a V_g approaching the drain bias (V_d), respectively. Based on the description of E in the OFET, it is viable to use this device structure to evaluate the field-assisted charge separation in the BHJ blends by examining the photoresponse under irradiation.

In this contribution, we study the photoresponse (under AM 1.5 G) and dark transport of two commonly used BHJs comprising of the donors of poly(3-hexylthiophene) (P3HT) and 3,6-bis(5-(benzofuran-2-yl)thiophen-2-yl)-2,5-bis(2-ethylhexyl)pyrrolo[3,4-c]pyrrole-1,4-dione (DPP(TBFu)$_2$) blended with [6,6]-phenyl-C70-butyric acid methyl ester ($PC_{70}BM$) acceptor using FET device structure (Figure 2). To mimic the solar cell operation, standardized AM 1.5G light was perpendicularly shined on top of the BHJ films with a calibrated light intensity of 100 mW/cm^2 (1 sun).

2. EXPERIMENTAL SECTION

Materials and Device Fabrication. Regioregular P3HT and $PC_{70}BM$ were purchased from Plextronic and Solenne BV, respectively, and used as received. DPP(TBFu)$_2$ was synthesized as previous report.[18] The chemical structures of the materials are drawn in Figure 2b−d.

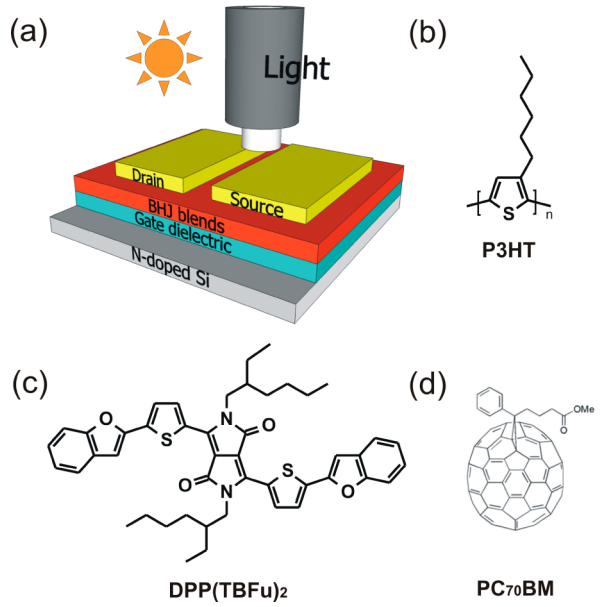

Figure 2. (a) FET device architecture with the illustrated light setup and chemical structures of (b) P3HT, (c) DPP(TBFu)$_2$, and (d) $PC_{70}BM$.

For sandwich-type solar cell devices, P3HT:$PC_{70}BM$ in a blend ratio of 55:45 was dissolved in chlorobenzene with a total concentration of 20 mg/mL. The DPP(TBFu)$_2$:$PC_{70}BM$ in a blend ratio of 60:40 were dissolved in chloroform with a total concentration of 17 mg/mL. Prior to the casting of active layers, 60 nm of poly(3,4-ethylenedioxythiophene) poly(styrenesulfonate) (PEDOT:PSS) layer was spin-coated on precleaned indium−tin-oxide (ITO) substrates and baked at 140 °C for 20 min. BHJ active layers were then deposited from the solutions using a spin-coater, leading to a thickness of typically 90 nm. The last step involved thermal evaporation of a 90 nm Al top contact.

For FET device fabrications, the active layers were cast from the same BHJ solutions used for the solar cell devices. Si/SiO_2 substrates were sonicated in acetone and isopropanol and then treated in the UV−O_3 oven for 30 min. Prior to the deposition of active layers, the Si/SiO_2 substrates were passivated by hexamethyldisilazane (HMDS) and then dried on a hot plate at 100 °C in a nitrogen-purged glovebox. Finally 90 nm of Au was evaporated on top of the BHJ layers through shadow masks, resulting in a FET channel length of 70 μm and channel width of 2 mm.

Device Characterization. Solar cell devices were thermal annealed on a hot plate for 10 min in the N_2 atmosphere at 140 °C for P3HT:$PC_{70}BM$ and 110 °C for DPP(TBFu)$_2$:$PC_{70}BM$. Standard solar cell characterizations were carried out in dry nitrogen environment under simulated 100 mW/cm^2 AM1.5G (1 sun) irradiation from a 300W Xe arc lamp with an AM 1.5 global filter. External quantum efficiencies (EQE) were measured with a monochromator, optical chopper, and lock-in amplifier sourced by a Xe lamp. Photon flux was determined by a NREL certified Si photodiode.

FET devices were thermally annealed to the same temperatures as for the solar cells. FET characterizations were performed in a Lakeshore probe station under a vacuum of ~1 × 10^{-6} mBar by using a Keithley 4200 semiconductor parametric analyzer. Impedance spectroscopy was recorded using a Solartron SI 1260 impedance/gain-phase analyzer. The simulated AM 1.5G light was shined through a quartz glass window on top of the FET channels with the irradiation intensity of ~100 mW/cm^2 calibrated by a photodiode.

3. RESULTS AND DISCUSSION

3.1. Solar Cell Device Characterizations. Figure 3a shows typical current density−voltage (J−V) characteristics of

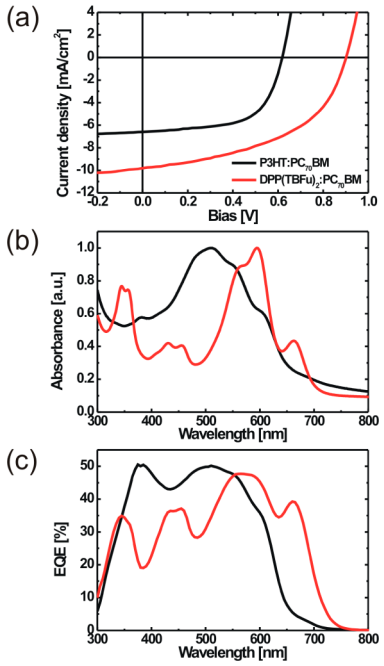

Figure 3. (a) Current density–voltage characteristics (J–V) of solar cell devices based on active layers comprising of P3HT:$PC_{70}BM$ (140 °C annealed), and DPP$(TBFu)_2$:$PC_{70}BM$ (110 °C annealed) under standardized AM 1.5 100 mW/cm^2 illumination. (b) UV–vis absorption spectra of the according P3HT:$PC_{70}BM$ and DPP$(TBFu)_2$:$PC_{70}BM$ thin films. (c) External quantum efficiency of the solar cell devices.

the devices comprising active layers of P3HT:$PC_{70}BM$ annealed at 140 °C and DPP$(TBFu)_2$:$PC_{70}BM$ annealed at 110 °C. The solar cell parameters upon AM 1.5G illumination are summarized in Table 1. A higher PCE of 4.3% is found for

Table 1. Parameters of Solar Cells Comprising Active Layer of P3HT:$PC_{70}BM$ Annealed at 140 °C and DPP$(TBFu)_2$:$PC_{70}BM$ Annealed at 110 °C under 100 mW/cm^{-2} Illumination

	J_{sc} (mA/cm^2)	V_{oc} (V)	*FF*	PCE (%)
P3HT:$PC_{70}BM$	6.6	0.62	0.61	2.5
DPP$(TBFu)_2$:$PC_{70}BM$	9.8	0.91	0.48	4.3

the DPP$(TBFu)_2$:$PC_{70}BM$ than the P3HT:$PC_{70}BM$ devices with PCE of 2.5%, owing to a relative high open-circuit voltage (V_{oc}) of 0.91 V and a large short-circuit current (J_{sc}) of 9.8 mA/cm^2. The deeper highest occupied molecular orbital (HOMO) of DPP$(TBFu)_2$ (5.2 eV) can be responsible for the higher V_{oc} as compared to the polymer device.[40,41] The high J_{sc} in addition to the smaller bandgap (1.7 eV) can be ascribed to forming a desirable nanoscale phase-separated film morphology upon thermal annealing at 110 °C.[42] However, the DPP$(TBFu)_2$:$PC_{70}BM$ device displays a low *FF* of 0.48 when compared to the P3HT:$PC_{70}BM$ device having a *FF* of 0.61, which is the major limiting factor for the efficiency. An earlier study on this DPP system has demonstrated that the reduction of *FF* is caused by a substantial charge recombination at light intensities approaching 1 sun.[25,32]

Figure 3b shows normalized thin-film UV–vis absorbance of the two BHJ blends prepared equivalently to the active layer for devices. Both films show an absorption in 300–400 nm region, which is attributed to the absorption of $PC_{70}BM$. Relative to the maximum donor absorption at 510 nm for P3HT:$PC_{70}BM$, DPP$(TBFu)_2$:$PC_{70}BM$ displays a 85 nm red-shifted donor absorption at 595 nm with resolved vibronic features. Additionally DPP$(TBFu)_2$:$PC_{70}BM$ displays a pronouncing shoulder absorption at 662 nm in comparison to that of P3HT:$PC_{70}BM$ appearing at 607 nm, indicative of strong aggregates formed in the solid-state films upon thermal annealing.[43,44] Figure 3c shows EQE spectra of these two solar cell devices. Integration of the EQE spectra agrees with the J_{sc} from J–V characteristics. The peaks of the EQE of P3HT:$PC_{70}BM$ and DPP$(TBFu)_2$:$PC_{70}BM$ devices are correlated well to their absorption peaks. On average the P3HT:$PC_{70}BM$ device shows a higher EQE (of ~50%) than DPP$(TBFu)_2$:$PC_{70}BM$ devices over the whole visible spectrum while the maximal EQE of the latter appears at 590 nm where the DPP$(TBFu)_2$ absorbs the most. The noticeable difference in the film absorption and the corresponding device EQE can be due to the difference in the film thickness and/or the charge generation, transport, and collection of the active layer. The absorption measures a photon absorption event whereas EQE measures the outcome of multiple processes in the device. These combined effects may lead to a low light penetration depth and the generated charge carriers cannot efficiently travel to the other side of the film toward the contact, thus hurting the collection efficiency.[45] Between the two systems, the larger J_{sc} of the DPP$(TBFu)_2$:$PC_{70}BM$ solar cell is ascribed to extended absorption into low energy photons, leading to an onset of the photocurrent at around 720 nm. The EQE of the DPP$(TBFu)_2$ device however decreases to 35% in the $PC_{70}BM$ absorption region when compared to P3HT devices. The reduction of EQE in this region indicates a lower charge conversion efficiency in the DPP$(TBFu)_2$:$PC_{70}BM$ blends when excitons are primarily created on the acceptor phase. A possible explanation might be due to the relatively large fullerene domains or the formation of isolated fullerene domains within the BHJ, which may affect the charge generation and charge transport, eventually reducing the change collection efficiency.[46–48]

3.2. FET Charge Transport and Photoresponse. To better understand the quantum efficiency and photocurrent generation in these devices, we examined the charge transport in the photoactive blends using FET structure. Figure 4a–f (symbols) display dark transfer (left panels) and output (right panels) characteristics based on active layers comprising the P3HT:$PC_{70}BM$ annealed at 140 °C and the DPP$(TBFu)_2$:$PC_{70}BM$ annealed at 110 °C, respectively with drain voltage $V_d = \pm 60$ V (for the transfer) and gate bias $V_g = \pm 60$ V (for the output). For both devices, the transfer curves exhibit a bipolar behavior, as manifested by the increase of the drain current (I_{ds}) with V_g at both p- and n-type modes. We observe a dominant p-type transport in P3HT:$PC_{70}BM$ blends over the n-type one, producing a dark hole mobility (μ_h) of 5.2×10^{-4} $cm^2/(V\ s)$ and an electron mobility (μ_e) of 2.2×10^{-5} $cm^2/(V\ s)$. The output curves with $V_g = \pm 60$ V for the P3HT:$PC_{70}BM$ FET in Figure 4b also display a larger hole current with a saturated $I_{ds} = 0.16$ μA for $V_{ds} = -50$ V and a saturated I_{ds} reduced to 0.02 μA in the n-type regime for $V_{ds} = 50$ V. In contrast, DPP$(TBFu)_2$:$PC_{70}BM$ shows a more asymmetric hole transport when compared to that of the electron, with $\mu_h = 8.2 \times 10^{-6}$ $cm^2/(V\ s)$ and $\mu_e = 1.3 \times 10^{-3}$ $cm^2/(V\ s)$ in dark. This trend is observed consistently by output curves (see Figure 4d) showing a saturated I_{ds} at 0.017 μA and at 0.47 μA in the p-type

dx.doi.org/10.1021/am302833j | ACS Appl. Mater. Interfaces 2013, 5, 2347–2353

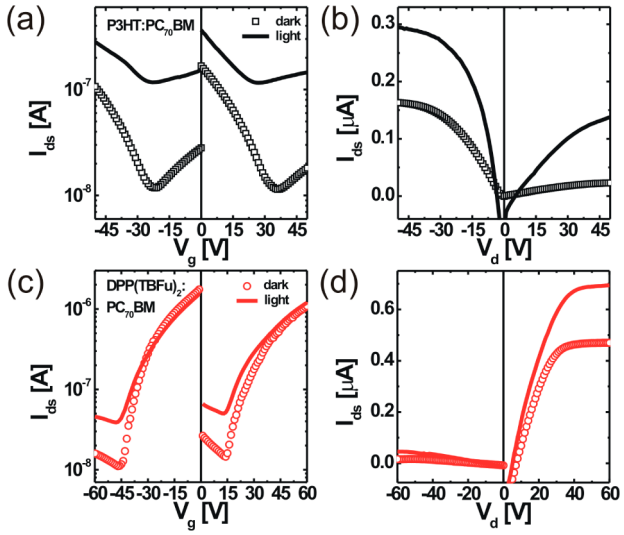

Figure 4. Transfer (left panels) and output (right panels) characteristics of field-effect transistors when measured in dark (open symbols) and under 100 mW/cm^{-2} illumination (lines) with V_g = ±60 V based on active layers of (a) P3HT:$PC_{70}BM$ annealed at 140 °C, and (c) $DPP(TBFu)_2$:$PC_{70}BM$ annealed at 110 °C.

and n-type regimes, respectively. The less balanced dark carrier mobility of the $DPP(TBFu)_2$:$PC_{70}BM$ blends can partially contribute to the lower *FF* observed in DPP solar cells shown in Figure 3a.

We also measured the hole mobility in pristine donor materials and BHJ blends. From the results shown in Figure S1 (see the Support Information, or SI), we notice that upon adding the $PC_{70}BM$ acceptor, the hole currents are reduced for both blend systems with μ_h decreasing from 4.7 × 10^{-3} cm^2/(V s) to 5.2 × 10^{-4} cm^2/(V s) for P3HT, and from 1.6 × 10^{-4} cm^2/(V s) to 8.2 × 10^{-6} cm^2/(V s) for $DPP(TBFu)_2$. The reduced hole transport when blended with the acceptor observed here is opposite to poly[2-methoxy-5-(3′,7′-dimethyloctyloxy)-1,4-phenylenevinylene]:PCBM where the hole mobility increases upon the addition of PCBM.[50]

Next we focus on studying the photoresponse of the two BHJ blends under irradiation. The lines in Figure 4a-d show transfer and output characteristics for the two devices when measured under 100 mW/cm^2 irradiation. In both p- and n-type modes, P3HT:$PC_{70}BM$ shows the utmost enhancement of the photoconductivity by displaying a large increase of I_{ds} at different V_g. Interestingly, the relatively low dark electron current can be recovered upon irradiation, from I_{ds} = 0.02 μA in dark to I_{ds} = 0.14 μA under 1 sun with V_g = 50 V. The electron current is now on the same order of the hole photocurrent of 0.29 μA for V_g = −50 V. This observation is further reflected by the output curves shown in Figure 4b (lines). The hole and electron currents (with V_g = ± 50 V) upon illumination are enhanced by 2 and 7 folds, respectively, approaching a balanced I_{ds}. From Figure 4c, the I_{ds} of the $DPP(TBFu)_2$:$PC_{70}BM$ device under irradiation also displays a 5-fold increase in the hole-dominating regimes for V_g < −45 and 0 V < V_g < 15 V. Conversely, one observes a nearly unchanged I_{ds} in electron-dominating for −45 V < V_g < 0 V and 15 V < V_g < +60 V (see Figure 4c) upon illumination. From the output curves shown in Figure 4d, $DPP(TBFu)_2$:$PC_{70}BM$ FET exhibits a relatively low enhancement of I_{ds} under irradiation, for example from 0.017 to 0.045 μA in the p-type mode and from 0.47 to 0.69 μA in the n-type mode for V_d = ± 50 V. $DPP(TBFu)_2$:$PC_{70}BM$ clearly show a weaker photoresponse along with much larger imbalance in transport properties upon irradiation. These observations to certain degree show a correlation with the observed lower *FF* and quantum efficiency of DPP solar cells. An imbalanced carrier mobility of the BHJ can lead to a redistribution of charge carriers, thus resulting in the undesirable space-charge effect[20] and a stronger charge recombination.[50]

3.3. Photocurrent Generation in OFETs. To establish the mechanism of the change in the FET characteristics and the resultant photocurrent (I_{photo}(FET)) upon irradiation, where I_{photo}(FET) is defined by,

$$I_{photo}(\text{FET}) = I_{ds}(\text{light}) - I_{ds}(\text{dark}) \quad (1)$$

we first measured the FET transfer curves under 100 mW/cm^2 illumination based on the two pristine donor materials and the results are shown in Figure S2 in the Supporting Information. It is obvious that the neat P3HT depicts a slightly enlarged I_{ds}, whereas the $DPP(TBFu)_2$ show an unchanged current or a zero I_{photo}(FET) without $PC_{70}BM$ acceptor. Therefore, the observed FET photoresponse of the two blends is primarily due to the exciton dissociation and charge transfer via the donor/acceptor interface in the BHJ.

The occurrence of I_{photo}(FET) shown in Figure 4 can be understood by the illustrations in Figure 1 for the OFET operated at the p-type or n-type mode. For example when running the OFET in the p-type mode with V_{ds} = −60 V, (see Figure 4a), the hole concentration in the conduction channel is low for a low V_g and then the FET is in the off-state. Upon irradiation, electron−hole pairs are generated in the entire BHJ active layer due to charge transfer.[51] Because of the presence of *E* as shown by the arrows in Figure 1, more electron−hole pairs are likely to be separated in the area laterally nearing the drain electrode where the *E* is stronger. Based on the bias polarity of the *E*, separated holes tend to drift toward the drain electrode leaving electrons moving toward the dielectric/semiconductor interface. As a consequence, an extra number of holes can be swept out by the drain electrode, contributing to the I_{photo}(FET). Similarly for the FET operated in the n-type mode with V_{ds} = 60 V, under a low V_g, more electron−hole pairs photogenerated in the BHJ film are likely to be separated laterally near the drain electrode. As a result, the extra electrons swept out by the electrode can contribute to the electron current, leading to a net I_{photo}(FET). On the basis of these two scenarios, the observed increase in I_{ds} of P3HT:$PC_{70}BM$ and $DPP(TBFu)_2$:$PC_{70}BM$ FETs at low V_g in panels a and c in Figure 4 can be rationalized.

When a FET is operated in the saturation regime with applying a large V_g (±60 V), the gate-induced carrier concentration becomes higher in the conduction channel. Based on the bias, the *E* can be approximated by those white arrows showed in Figure 1c and 1d. In these situations, this field can also contribute to the separation of light-induced electron−hole pairs upon irradiation. Differently the I_{photo}(FET) in this regime is mainly dictated by the photovoltaic effect and it is given by,[52]

$$I_{photo}(\text{FET}) = A\frac{k_B T}{q}\ln\left(1 + \frac{\eta q \lambda P_{light}}{I_{dark} hc}\right) \quad (2)$$

where *A* is a prefactor, η is the external quantum efficiency, *q* is the elementary charge, P_{light} is the incident light power, I_{dark} is

the dark current and hc/λ represents the photon energy. In contrast to the scenario depicted in panels a and b in Figure 1, carrier concentration induced by V_g is typically of ~1×10^{18} to 1×10^{19} cm^{-3} when a FET is turned on.[53] This can be orders higher than the free carrier density introduced by photoabsorption. In addition, further increase of the V_g may give rise to an increased possibility for the charge recombination between photoinduced and surface trapped charge carriers,[54] further limiting the I_{photo}(FET). Under such conditions, the V_g induced charge carriers are dominant for the current in the OFET. In principle, I_{ds} should be less sensitive to the light when compared to the low V_g regime. However the higher photoresponse of P3HT:$PC_{70}BM$ observed in this regime can suggest that a larger number of photoinduced carriers can be generated in the active layer. Because the E can be strongly changed with V_g, the larger photoresponse regardless of the V_g implies that charge separation in P3HT:$PC_{70}BM$ might be less field-dependent than the DPP(TBFu)$_2$:$PC_{70}BM$. Another possible effect is the relatively high photosensitivity in the pristine P3HT (see Figure S2 in the Supporting Information).

3.4. Photogenerated Carrier Density in OFETs. At last, we determine the photogenerated carrier concentration (ρ_{photo}) upon irradiation in the FET and compare to that achieved in according solar cell devices under operation. Figure 5a shows

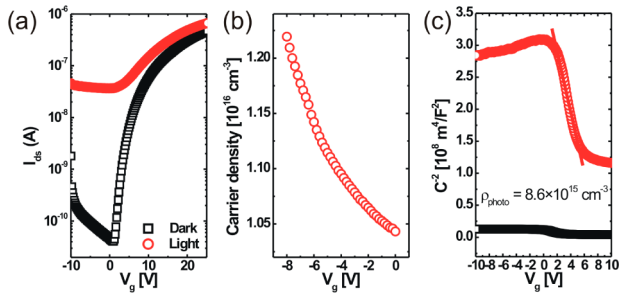

Figure 5. (a) Comparison of the dark and illuminated transfer characteristics of the DPP(TBFu)$_2$:$PC_{70}BM$ FET under the *n*-type accumulation with V_d = 20 V. (b) Photoinduced carrier concentration in the DPP(TBFu)$_2$:$PC_{70}BM$ film determined from panel a. (c) Carrier concentration extracted by impedance spectroscopy on the same device measured in dark (black squares) and under 100 mW/cm^2 illumination (red circles), respectively.

dark and illuminated FET transfer characteristics of DPP(TBFu)$_2$:$PC_{70}BM$ with V_{ds} = 20 V for the device operated in the linear regime. The reason of choosing a low V_{ds} is to minimize the influence from charge injection so that the difference in I_{ds} after irradiation can be attributed mostly to the photoresponse. The ρ_{photo} is determined by the I_{photo}(FET) using the followed equations,[55]

$$\rho_{photo} = \frac{L}{m_{h,e} q \mu_{h,e} W d V_d} I_{photo}(\mathrm{FET}) \tag{3}$$

$$m_h = 1 + \mu_n/\mu_p$$

$$m_e = 1 + \mu_p/\mu_n \tag{4}$$

where L, W, and d is the FET channel length, channel width, and film thickness, respectively, q is the elementary charge, and $\mu_{h,e}$ is the FET hole or electron mobility in dark. Figure 5b shows the extracted ρ_{photo} as a function of V_g. The ρ_{photo} falls in the range of ~1×10^{16} cm^{-3} showing a lightly increase from 1 $\times 10^{16}$ cm^{-3} to 1.2 $\times 10^{16}$ cm^{-3} with V_g decreasing from 0 V to −8 V. This is due to the enhancement of the vertical E close to the drain electrode as depicted in Figure 1b. In order to validate the ρ_{photo} determined based on this method, impedance analysis was performed on the same FET device. Figure 5c shows the obtained capacitance (C) in dark and upon irradiation as a function of V_g, respectively. The C is greatly enhanced upon irradiation, which is mainly due to the enhancement of ρ_{photo} in the photoactive layer. Besides C displays a sharp decrease for 0 V < V_g < 6 V where light-induced carriers are being depleted by the V_g. Using the equation given by[56]

$$\frac{1}{C^2} = \frac{1}{C_{ox}} + \frac{2}{\varepsilon_0 \varepsilon_r q \rho_{photo}} V_g$$

$$\rho_{photo} = \frac{2}{q \varepsilon_0 \varepsilon_r \left(\frac{d(1/C^2)}{dV_g} \right)} \tag{5}$$

where C_{ox} is the capacitance of the gate dielectric, and ε_r is the dielectric constant of the active layer, we obtain a ρ_{photo} of 8.6 × 10^{15} cm^{-3} for the DPP(TBFu)$_2$:$PC_{70}BM$ blend. The results of ρ_{photo} determined with eqs 4 and 5 are comparable and this can ensure the applicability of these two analysis methods. Similarly, we obtain a ρ_{photo} of 7.8 × 10^{16} cm^{-3} for the P3HT:$PC_{70}BM$ blend using the FET analysis based in Figure 4a.

Now we compare the ρ_{photo} obtained using FET analysis to the carrier density generated in the solar cells, which shows a ρ_{photo} of 4.4 × 10^{16} cm^{-3} and 6.9 × 10^{16} cm^{-3} for DPP(TBFu)$_2$:$PC_{70}BM$ and P3HT:$PC_{70}BM$, respectively at 1 sun.[25] The carrier density in solar cells was measured previously using impedance spectroscopy under illumination.[25] Under the same irradiation intensity, the ρ_{photo} in DPP(TBFu)$_2$:$PC_{70}BM$ solar cells is roughly 4 times higher than the carrier density in the OFET. In contrast, we observe a similar ρ_{photo} of the P3HT:$PC_{70}BM$ blends for both device structures, solar cells and FETs. Although the transistor and solar cell have distinctions in the charge transport directionality, electric field, and the photoabsorption by the active layer, the results help us further understanding the influence of E on the charge separation. Besides it can imply that the field-dependence of the charge separation in the DPP(TBFu)$_2$:$PC_{70}BM$ is like to be to stronger than that in the P3HT:$PC_{70}BM$ blends. The photoresponse along with its field-dependence in the OFET to certain degree can be linked to the solar cell performance presented in Figure 3. For the DPP(TBFu)$_2$:$PC_{70}BM$, on top of the effect of the charge transport, and recombination, etc., the larger field-dependence of the charge separation can also contribute to the stronger bias dependence of the photocurrent in the solar cell and thus the J−V characteristics exhibit a relatively poor *FF*.

4. CONCLUSION

To conclude, we investigated the device performance of polymer and small molecule solution-processed BHJ solar cells and the photoresponse and dark transport using OFETs. The field-dependence of the photoresponse can be correlated with the process of charge separation, which is field-assisted. For P3HT:$PC_{70}BM$, a more balanced carriers mobility, the weaker field-dependence of the charge separation and higher photoresponse can contribute to the higher quantum efficiency and *FF* observed on the solar cell device. As contrary, the

dx.doi.org/10.1021/am302833j | ACS Appl. Mater. Interfaces 2013, 5, 2347−2353

DPP(TBFu)$_2$:PC$_{70}$BM exhibits a large imbalanced dark carriers mobility, a stronger field-dependent charge generation and a weaker photoresponse. These behaviors lead to the poor *FF* and quantum efficiency in DPP(TBFu)$_2$ solar cells. We demonstrate that FET device structure is a useful tool for understanding the effect of field-dependent charge generation and charge transport on solar cell performance.

■ ASSOCIATED CONTENT

Supporting Information

Hole mobility in pristine donor materials and BHJ blends and photoresponse of pristine P3HT and DPP(TBFu)$_2$. This material is available free of charge via the Internet at http://pubs.acs.org/.

■ AUTHOR INFORMATION

Corresponding Author

*E-mail: quyen@chem.ucsb.edu.

Notes

The authors declare no competing financial interest.

■ ACKNOWLEDGMENTS

This work is supported by the Office of Naval Research (N00014-11-1-0255). TQN thanks the Camille Dreyfus Teacher Scholar Award and the Alfred Sloan Research Fellowship program. The authors thank Dr. Martijn Kuik (University of California, Santa Barbara) for helpful discussion.

■ REFERENCES

(1) Lloyd, M. T.; Anthony, J. E.; Malliaras, G. G. *Mater. Today* **2007**, *10*, 34.

(2) Natalie, S. S.; Smits, E.; Wondergem, H.; Tanase, C.; Blom, P. W .M.; Smith, P.; de Leeuw, D. *Nat. Mater.* **2005**, *4*, 601.

(3) Mayeröffer, U.; Deing, K.; Gruß, K.; Braunschweig, H.; Meerholz, K.; Würthner, F. *Angew. Chem., Int. Ed.* **2009**, *48*, 8776.

(4) Imahori, H.; Fukuzumi, S. *Adv. Funct. Mater.* **2004**, *14*, 525.

(5) Peumans, P.; Yakimov, A.; Forrest, S. R. *J. Appl. Phys.* **2003**, *93*, 3693.

(6) Silvestri, F.; Irwin, M. D.; Beverina, L.; Facchetti, A.; Pagani, G. A.; Marks., T. J. *J. Am. Chem. Soc.* **2008**, *130*, 17640.

(7) Welch, G. C.; Perez, L. A.; Hoven, C. V.; Zhang, Y.; Dang, X. D.; Sharenko, A.; Toney, M. F.; Kramer, E. J.; Nguyen, T.-Q.; Bazan, G. C. *J. Mater. Chem.* **2011**, *21*, 12700.

(8) Schmidt-Mende, L.; Fechtenkötter, A.; Müllen, K.; Moons, E.; Friend, R. H.; MacKenzie, J. D. *Science* **2001**, *293*, 1119.

(9) Roquet, S.; Cravino, A.; Leriche, P.; Alévêque, O.; Frère, P.; Roncali, J. *J. Am. Chem. Soc.* **2006**, *128*, 3459.

(10) Ma, C. Q.; Fonrodona, M.; Schikora, M. C.; Wienk, M. M.; Janssen, R. A. J.; Bäuerle, P. *Adv. Funct. Mater.* **2008**, *18*, 3323.

(11) Sun, Y.; Welch, G. C.; Leong, W. L.; Takacs, C. J.; Bazan, G. C.; Heeger, A. J. *Nat. Mater.* **2012**, *11*, 44.

(12) Lee, O. P.; Yiu, A. T.; Beaujuge, P. M.; Woo, C. H.; Holcombe, T. W.; Millstone, J. E.; Douglas, J. D.; Chen, M. S.; Fréchet, J. M. J. *Adv. Mater.* **2011**, *23*, 5359.

(13) Li, Z.; He, G.; Wan, X. J.; Liu, Y. S.; Zhou, J. Y.; Long, G. K.; Zuo, Y.; Zhang, M. T.; Chen, Y. S. *Adv. Energy Mater.* **2012**, *2*, 74.

(14) Liu, Y. S.; Wan, X. J.; Wang, F.; Zhou, J. Y.; Long, G. K.; Tian, J. G.; Chen, Y. S. *Adv. Mater.* **2011**, *23*, 5387.

(15) Liu, Y. S.; Wan, X. J.; Wang, F.; Zhou, J. Y.; Long, G. K.; Tian, J. G.; You, J. B.; Yang, Y.; Chen, Y. S. *Adv. Energy Mater.* **2011**, *1*, 771.

(16) Loser, S.; Bruns, C. J.; Miyauchi, H.; Ortiz, R. P.; Facchetti, A.; Stupp, S. I.; Marks, T. J. *J. Am. Chem. Soc.* **2011**, *133*, 8142.

(17) Wei, G. D.; Wang, S. Y.; Sun, K.; Thompson, M. E.; Forrest, S. R. *Adv. Energy Mater.* **2011**, *1*, 184.

(18) Walker, B.; Tomayo, A. B.; Dang, X. D.; Zalar, P.; Seo, J. H.; Garcia, A.; Tantiwiwat, M.; Nguyen, T.-Q. *Adv. Funct. Mater.* **2009**, *19*, 3063.

(19) Tantiwiwat, M.; Tamayo, A.; Luu, N.; Dang, X. D.; Nguyen, T.-Q. *J. Phys. Chem. C* **2008**, *112*, 17402.

(20) Mihailetchi, V. D.; Wildeman, J.; Blom, P. W. M. *Phys. Rev. Lett.* **2005**, *64*, 126602.

(21) Blom, P. W. M.; Mihailetchi, V. D.; Koster, L. J. A.; Markov, D. E. *Adv. Mater.* **2007**, *19*, 1551.

(22) Fabiano, S.; Chen, Z.; Vahedi, S.; Facchetti, A.; Pignataro, B.; Loi, M. A. *J. Mater. Chem.* **2011**, *21*, 5891.

(23) Li, G.; Shrotriya, V.; Huang, J. S.; Yao, Y.; Moriarty, T.; Emery, K.; Yang, Y. *Nat. Mater.* **2005**, *4*, 864.

(24) Andersson, L. M.; Müller, C.; Badada, B. H.; Zhang, F. L.; Würfel, U.; Inganäs, O. *J. Appl. Phys.* **2011**, *110*, 024509.

(25) Zhang, Y.; Dang, X. D.; Kim, C.; Nguyen, T.-Q. *Adv. Energy Mater.* **2011**, *1*, 610.

(26) Credginton, D.; Jamieson, F. C.; Walker, B.; Nguyen, T.-Q.; Durrant, J. R. *Adv. Mater.* **2012**, *24*, 2135.

(27) Proctor., C.; Kim, C.; Nguyen, T.-Q. "Nongeminate Recombination and Charge Transport Limitations in Diketopyrrolopyrrole Based Solution Processed Small Molecule Solar Cells". *Adv. Funct. Mater.* in press.

(28) Chance, R. R.; Braun, C. L. *J. Chem. Phys.* **1976**, *64*, 3573.

(29) Borsenberger, P. M.; Ateya, A. I. *J. Appl. Phys.* **1978**, *49*, 4035.

(30) Kniepert, J.; Schubert, M.; Blakesley, J. C.; Neher, D. *J. Phys. Chem Lett.* **2011**, *2*, 700.

(31) Credgington, D.; Hamilton, R.; Atienzar, P.; Nelson, J.; Durrant, J. R. *Adv. Funct. Mater.* **2011**, *21*, 2744.

(32) Gulbinas, V.; Zaushitsyn, Y.; Sundström, V.; Hertel, D.; Bässler, H.; Yartsev, A. *Phys. Rev. Lett.* **2002**, *89*, 107401.

(33) Veldman, D.; Ipek, Ö.; Meskers, S. C. J.; Sweelssen, J.; Koetse, M. M.; Veenstra, S. C.; Kroon, J. M.; van Bavel, S. S; Loos, J.; Janssen, R. A. J. *J. Am. Chem. Soc.* **2008**, *130*, 7721.

(34) Horowitz, G. *Adv. Mater.* **1998**, *10*, 365.

(35) Morana, M.; Koers, P.; Waldauf, C.; Koppe, M.; Muehlbacher, D.; Denk, P.; Scharber, M.; Waller, D.; Brabec, C. *Adv. Funct. Mater.* **2007**, *17*, 3274.

(36) Bürgi, L.; Sirringhaus, H.; Friend, R. H. *Appl. Phys. Lett.* **2002**, *80*, 2913.

(37) Smits, E. C. P.; Mathijssen, S. G. J.; Cölle, M.; Mank, A. J. G.; Bobbert, P. A.; Blom, P. W. M.; de Boer, B.; de Leeuw, D. M. *Phys. Rev. B* **2007**, *76*, 125202.

(38) Weis, M.; Manaka, T.; Iwamoto, M. *J. Appl. Phys.* **2009**, *105*, 024505.

(39) Manaka, T.; Lim, E.; Tamura, R.; Yamada, D.; Iwamoto, M. *Appl. Phys. Lett.* **2006**, *89*, 072113.

(40) Chen, H. Y.; Hou, J. H.; Zhang, S. Q.; Liang, Y. Y.; Yang, G. W.; Yang, Y.; Yu, L. P.; Wu, Y.; Li, G. *Nat. Mater.* **2009**, *3*, 649.

(41) Vandewal, K.; Tvingstedt, K.; Gadisa, A.; Inganäs, O.; Manca, J. V. *Nat. Mater.* **2009**, *8*, 904.

(42) Peet, J.; Kim, J. Y.; Coates, N. E.; Ma, W. L.; Moses, D.; Heeger, A. J.; Bazan, G. C. *Nat. Mater.* **2007**, *6*, 497.

(43) Chivase, D.; Parisi, J.; Hummelen, J. C.; Dyakonov, V. *Nanotechnology* **2004**, *15*, 1317.

(44) Erb, T.; Zhokhavets, U.; Gobsch, G.; Raleva, S.; Stühn, B.; Schilinsky, P.; Waldauf, C.; Brabec, C. J. *Adv. Funct. Mater.* **2005**, *15*, 1193.

(45) Cabanillas-Gonzalez, J.; Yeates, S.; Bradley, D. D. C. *Synth. Met.* **2003**, *139*, 637.

(46) Mikhnenko, O. V.; Azimi, H.; Scharber, M.; Morana, M.; Blom, P. W. M.; Loi, M. A. *Energy Environ. Sci.* **2012**, *5*, 6960.

(47) Mikhnenko, O. V.; Lin, J.; Shu, Y.; Anthony, J. E.; Blom, P. W. M.; Nguyen, T.-Q.; Loi, M. A. *Phys. Chem. Chem. Phys.* **2012**, 14.

(48) Qin, D.; Gu, P.; Dhar, R. S.; Razavipour, S. G.; Ban, D. *Phys. Status Solidi A* **2011**, *208*, 1967−1971.

(49) Tuladhar, S. M.; Poplavskyy, D.; Choulis, S. A.; Durrant, J. R.; Bradley, D. D. C.; Nelson, J. *Adv. Funct. Mater.* **2005**, *15*, 1171.

(50) Albrecht, S.; Schindler, W.; Kurpiers, J.; Kniepert, J.; Blakesley, J. C.; Dumsch, I.; Allard, S.; Fostiropoulos, K.; Scherf, U.; Neher, D. *J. Phys. Chem. Lett.* **2012**, *3*, 640.
(51) Yu, G.; Gao, J.; Hummelen, J. C.; Wudl, F.; Heeger, A. J. *Science* **1995**, *270*, 1789.
(52) Kang, H.-S.; Choi, C. S.; Choi, W.-Y.; Kim, D.-H.; Seo, K.-W. *Appl. Phys. Lett.* **2004**, *84*, 3780.
(53) Tanase, C.; Meijer., E. J.; Blom, P. M. W.; de Leeuw, D. M. *Phys. Rev. Lett.* **2003**, *91*, 216601.
(54) Marjanović, N.; Singh, Th. B.; Dennler, G.; Günes, S.; Neugebauer, H.; Sariciftci, N. S.; Schwödiauer, R.; Bauer, S. *Org. Electron.* **2006**, *7*, 188.
(55) Wang, X.; Wasapinyokul, K.; Tan, W. D.; Rawcliffe, R.; Campbell, A. J.; Bradley, D. D. C. *J. Appl. Phys.* **2010**, *107*, 024509.
(56) Meijer, E. J.; Detcheverry, C.; Baesjou, P. J.; van Veenendaal, E.; de Leeuw, D. M.; Klapwijk, T. M. *J. Appl. Lett.* **2003**, *93*, 4831.